CASL-U-2013-0096-000

Power uprates
and plant life extension

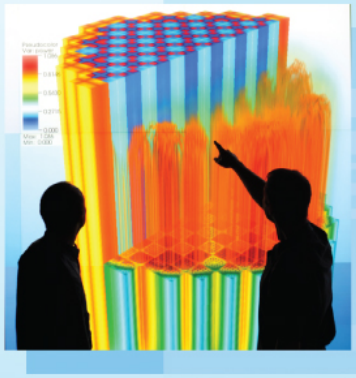

Engineering design
and analysis

Science-enabling
high performance
computing

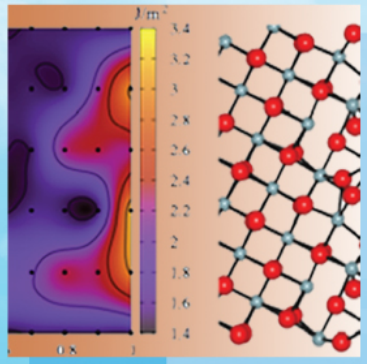

Fundamental science

Plant operational data

Consortium for Advanced Simulation of LWRs

Impact of 3D Spatial Variations in Fluid Flow on the Prediction of CRUD Deposition in a 4X4 PWR Sub-Assembly

University of Michigan and Los Alamos National Laboratory

V. Petrov, Brian K. Kendrick, Daniel Walter, and Annalisa Manera

May 12-17, 2013:

U.S. DEPARTMENT OF ENERGY | Nuclear Energy

IMPACT OF 3D SPATIAL VARIATIONS IN FLUID FLOW ON THE PREDICTION OF CRUD DEPOSITION IN A 4X4 PWR SUB-ASSEMBLY

Victor Petrov[1], Brian K. Kendrick[2], Daniel Walter[1], Annalisa Manera[1]
[1] Department of Nuclear Engineering & Radiological Sciences, University of Michigan, MI, USA
[2] Los Alamos National Laboratory, Los Alamos, NM, USA

petrov@umich.edu, bkendric@lanl.gov, djwalter@umich.edu, manera@umich.edu

ABSTRACT

Crud deposition is responsible for clad wall thinning in PWR fuel rods, leading to so-called crud-induced localized corrosion (CILC) failures. The prediction of these occurrences requires a detailed modeling of local thermo-hydraulics and chemistry phenomena. Within the framework of a collaboration between the University of Michigan and the Los Alamos National Laboratory (LANL), the commercial computational fluid-dynamics (CFD) code STAR-CCM+ has been coupled with the macroscale chemistry code MAMBA in order to investigate the impact of local fluid dynamics parameters on the prediction of crud deposition. In a previous work, the detailed pin-by-pin power distribution of a Combustion Engineer PWR core was obtained using the neutron transport code DeCART coupled with the computational fluid dynamic (CFD) code STAR-CCM+. The obtained power distribution includes the azimuthal power variation within each single pin. A 4x4 sector out of the core hot fuel assembly has been selected as region of interest for the current investigation. The 4x4 sub-region has been chosen such as to include hot pins, and to have strong power variations in space both from pin to pin as well as azimuthally within a single pin. This is achieved by including pins located in the proximity of water rods and burnable absorbers. The results obtained with the coupled STAR-CCM+/MAMBA code demonstrate the impacts of grid-spacer-induced swirling flow on: (1) the location of hot spots on the fuel cladding, and (2) erosion of the crud layer due to surface shear stresses. These two effects are primarily responsible for the formation of the characteristic crud striping patterns observed on PWR fuel rods.

1. INTRODUCTION

It is well known that for PWRs (pressurized water reactors) the main contribution to the corrosive release of nickel and iron solubles and particulates within the main circuit loop arises from the various materials used in the construction of the reactor coolant system including carbon steel, iron-chrome-nickel alloys, stainless steels and nickel based alloys [1]. These corrosion products can then deposit on cladding surfaces, especially in the regions where subcooled nucleate boiling occurs. The deposits are called CRUD (Chalk River Unidentified Deposits), which refers to the reactor where they were first observed [1,2,3,4,5,6,7]. CRUD contains mostly nickel ferrite, nickel oxide, and nickel metal with other nickel-iron-chrome crystals. It has a porous structure, which can lead to significant boron and lithium absorption due to the subcooled boiling taking place within the pores. Since boron has a very high neutron

capture cross section, even small amounts can lead to the so-called axial offset anomaly (AOA), also referred to as crud induced power shift (CIPS), experienced on more than 16 PWRs in the USA and abroad [4,8]. Due to AOA/CIPS, affected power plants often have to be operated at reduced power levels, and ultrasonic cleaning techniques need to be applied in order to remove crud from the fuel rods during scheduled outages [9]. In view of these considerations and in order to improve and increase the economics of nuclear power plants operation, there is a need for a better understanding of the coupled phenomena associated with fluid flow and CRUD build-up and erosion.

2. MODEL DESCRIPTION

2.1 STAR-CCM+ model

The model used for the present study consists of a 4x4 sub-assembly selected from an existing quarter core simulation of a Combustion Engineering PWR previously performed at the University of Michigan by means of DeCART/STAR-CCM+ [10]. The 4x4 sub-region has been chosen such as to include the core hot pins, and to have strong power variations in space, both from pin to pin as well as azimuthally within a single pin. This is achieved by including pins located in the proximity of water rods and burnable absorbers, as shown in Figure 1. The power distribution, computed with the neutron transport code DeCART, was supplied to STAR-CCM+ in the form of a table containing the volumetric power [W/m^3] as a function of the spatial coordinates X[m], Y[m], and Z[m], as shown in Figure 2.

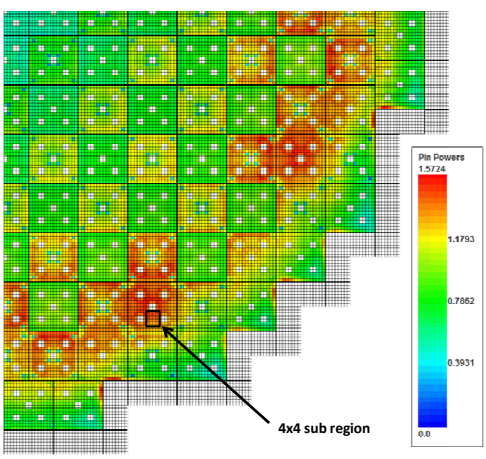

Figure 1 – Selected 4x4 sub-region from quarter core simulation by Kochunas et al., 2012 [10]

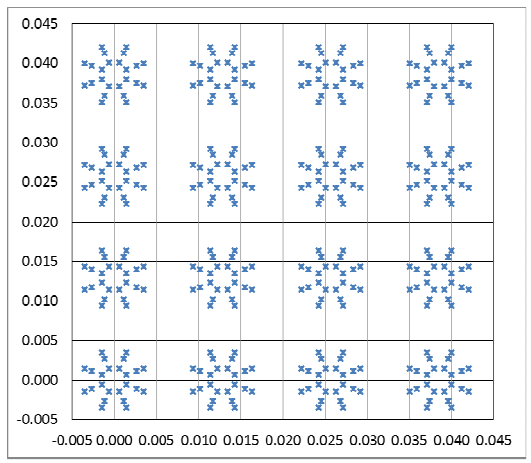

Figure 2 – Volumetric power mapping points.

The computational cost of the CFD model for the coolant flow in the fuel assembly is basically driven by the detailed mesh in the spacer grid regions. A typical PWR fuel bundle includes ten spacer grids. In order to reduce the computational cost associated to the CFD simulation, it was decided to explicitly model only three grid spacers out of ten. The three grid spacers included in the CFD model are the ones located where the highest cladding temperatures are expected. The locations of the spacers included in the CFD model are shown in figure 3. The actual spacer geometry was built following the specifications presented by Navarro and Santos [11]. According to these specifications, the central fuel pins are surrounded by two vanes each, while

peripheral fuel pins have no vanes present on the external sides of the grid spacer. The spacers have a height of 40 mm, and a wall thickness of 0.48 mm. A summary of the spacer, cladding and fuel pins dimensions is presented in Table 1, while in figure 4 the geometrical configuration of the spacer is presented. Since the goal of the current study was to demonstrate a proof-of-concept for a coupled simulation between CFD and the CRUD chemistry, some of the grid spacer geometrical details, such as springs windows and gaps, were excluded from the CFD model, in order to save computational power and time. These omitted details are not expected to play a role in the prediction of CRUD deposition.

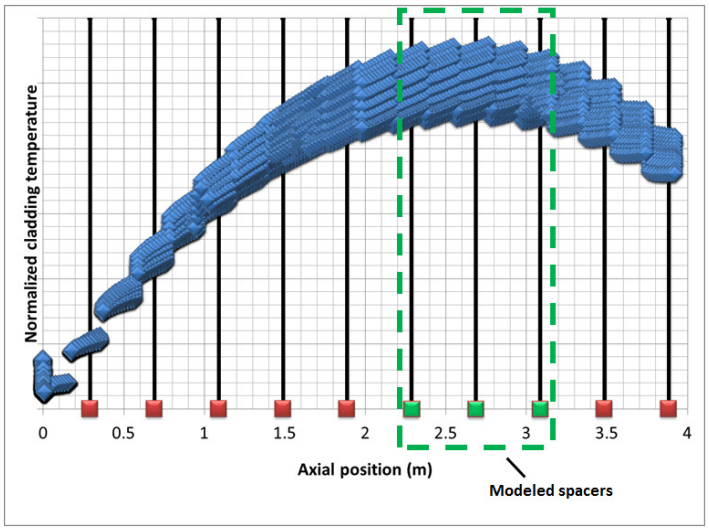

Figure 3 – Modeled spacer locations.

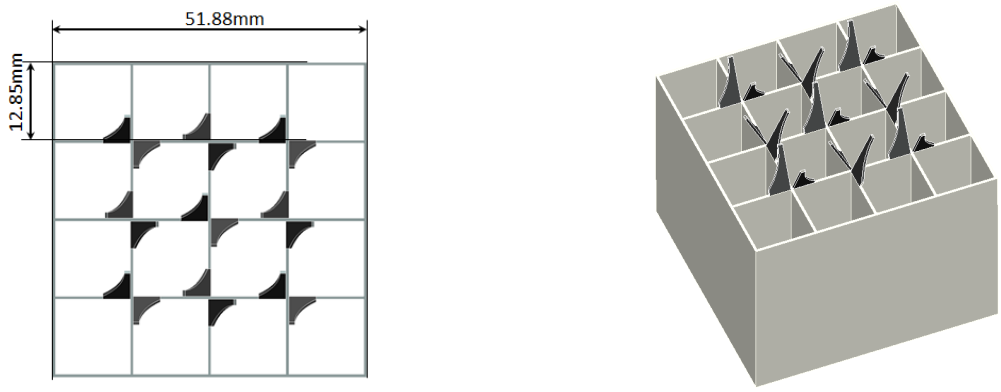

Figure 4 – Grid spacer geometry

Table 1 – Basic Geometry Data [10]

Parameter	Value (cm)
Pin pitch	1.285
Fuel rod outer radius	0.48515
Fuel pellet outer radius	0.42165
Active fuel height	393.02353

STAR-CCM+ was used for the CFD simulations. This is a commercial code [13] that solves the transport equations for continuity, 3-D momentum, and enthalpy on a very fine 3-D mesh. STAR-CCM+ is capable of modeling conjugate heat transfer, such that the conduction process is modeled within the fuel pellet and cladding, and the convective heat transfer is modeled in the cooling fluid that surrounds the pin. There are several options for modeling turbulent momentum and energy transport available in STAR-CCM+. The Reynolds-Averaged Navier-Stokes (RANS) approach for the solution of the k-ε transport equations was used in the present work for the modeling of turbulence. The computational mesh was built using the STAR-CCM+ polyhedral mesh generator for a single 4x4 grid spacer, and was then assembled using the STAR-CD mesh manipulation tools, in order to include all three grid spacers. In table 2 the number of cells in the computational domain is summarized separately for each region of the model (fuel, coolant and cladding, respectively). Details of the computational mesh are shown in figure 5.

Table 2 – Mesh details

	Cells	Faces
Cladding	8596085	36794712
Fuel	7277989	46693660
Coolant	15409550	83838283
Total	31283624	167326655

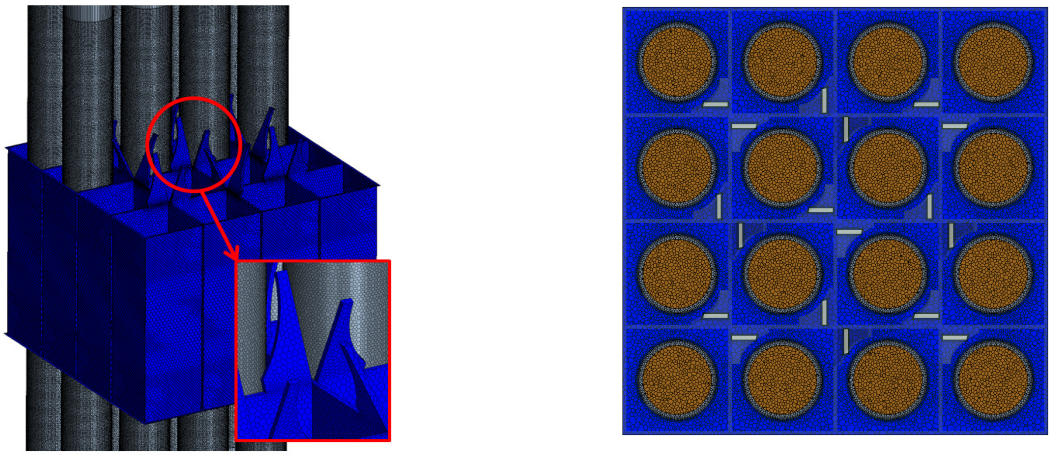

Figure 5 – Computational CFD mesh: isometric view (left), horizontal section view (right).

The Properties of the solid media (fuel and cladding) were considered to be constant and equal to the values reported in table 3. Since the variation of fluid properties within the investigated temperature ranges is significant, these were estimated by using the NIST steam/water tables [12], and interpolated applying polynomials of different orders for density (1) and viscosity (2), or by unilinear ratio expressions for specific heat (3) and thermal conductivity (4). In order to avoid the occurrence of unphysical fluid properties during the progression of the simulation, the fluid properties were limited by the values of the fluid properties at saturation. The system pressure was set equal to 155 bar. The flow boundary conditions were applied according to the specifications given in Ref. [10]: for the inlet condition, a uniform velocity of 5.278 m/s and a fluid temperature of 542.5 °F (299.61 °C) were used. At the assembly sides, symmetry boundary conditions were employed, while a pressure boundary was imposed at the outlet.

Table 3 – Thermo-physical Properties of Materials.

Material	Property	Value
Fuel	Density [kg/m3]	10400.0
	Specific Heat [J/kg-K]	300.0
	Thermal Conductivity [W/m-K]	6.0
Fuel Rod Cladding	Density [kg/m3]	6500.0
	Specific Heat [J/kg-K]	350.0
	Thermal Conductivity [W/m-K]	17.0

$$\rho(T) = -1670.325859 - 4.84697*\mathrm{T} + 0.01225*\mathrm{T}^2 - 1.16905*10^{-5}*T^3, \quad \rho_{sat} = 594.17\frac{kg}{m^3} \tag{1}$$

$$\mu(T) = 3.111 + 0.03026*T - 0.8131*10^{-4}*T^2 + 0.4635*10^{-7}*T^3 + 1.677*10^{-9}*T^4 - 0.3094*10^{-12}*T^5 + 0.151*10^{-15}*T^6, \quad \mu_{sat} = 7.287*10^{-5}\frac{Pa}{s} \tag{2}$$

$$c_p(T) = \frac{T - 59160}{-167.5 + 4.091*10^{-4}*T^2} + 3659, \quad c_{p_{sat}} = 8513\frac{J}{kg*K} \tag{3}$$

$$k(T) = \frac{0.1183*10^{12} + 0.2419*10^{9}*T}{1 - 0.4177*10^{13}*T + 0.138*10^{11}*T^2}, \quad k_{sat} = 0.45833\frac{W}{m*K} \tag{4}$$

2.2 MAMBA model

MAMBA (MPO Advanced Model for Boron Analysis) is a FORTRAN based computer code which simulates three-dimensional crud growth along the surface of a single fuel rod. MAMBA is being developed within the MPO (Materials Performance and Optimization) focus area of CASL.[7] The primary coupled physics and chemistry associated with crud formation that are currently treated in MAMBA include: (1) solving a general non-linear 3D heat transport equation for the crud layer including localized heat sinks due to the internal boiling within the crud layer, (2) an adaptive grid which grows radially in time as mass deposits on the surface of the crud, (3) time evolving microstructure (porosity) of the crud layer due to localized deposition and precipitation of nickel ferrite ($NiFe_2O_4$) and lithium tetraborate ($Li_2B_4O_7$) within the pores of the crud, (4) time evolving nickel, iron, lithium, and boric acid coolant chemistry both at the crud surface and inside the pores of the crud, (5) mass transport of various soluble coolant species into the interior of the crud due to boiling induced Darcy flow, (6) diffusion of various soluble species inside the crud due to the flow induced concentration gradients within the crud layer, and (7) mass evaporation in the form of steam vapor due to the localized boiling inside the crud layer. MAMBA utilizes a cylindrical coordinate system (r, θ, z) and is capable of simulating crud deposition along the entire surface of a 400 cm long fuel rod. It can also "zoom in" and treat selected regions of the fuel rod in high resolution. MAMBA can be run in stand alone mode or in coupled mode with a neutronics and thermal hydraulics/CFD code. The crud surface deposition rate is governed by two rate parameters, one for boiling regions which is multiplied

by the local mass evaporation rate (i.e., the steaming flux leaving the boiling chimneys), and one for non-boiling regions. In boiling regions, the crud growth rate is enhanced due to the boiling induced flow of coolant into the crud's surface which increases the flux of particulates onto the crud's surface. The crud surface deposition rate also includes a user selectable option for including an erosion (loss) term which is currently chosen to be proportional to the STAR-CCM+ computed turbulent kinetic energy. This empirical erosion model accounts for the local shear forces due to turbulent flow acting on and dislodging some of the crud's surface particles.[14,15] More advanced erosion models are being developed based on higher fidelity CFD methods, and may also include adhesion/strength models[16] for the crud's surface layer as well as other "release" mechanisms such as that due to sub-cooled boiling on and within the crud. Validation of these erosion models may be possible using a single-rod autoclave experiment such as the Westinghouse WALT Loop.[17]

The coolant chemistry is supplied by the user or an ex-core model (i.e., EPRIs BOA code[18]) and consists of the standard inputs: (1) boron concentration (ppm), (2) lithium concentration (ppm), (3) H_2 concentration (cc/Kg), (4) soluble Ni (ppb), (5) soluble Fe (ppb), and (6) particulate NiFe2O4 concentration (ppb). The thermodynamics of the coolant chemistry and the various precipitation parameters for the nickel-ferrite and boron species are currently based on EPRI's MULTEQ correlations (as used in BOA).[18] Future versions of MAMBA will also include the new thermodynamic models being developed within CASL. The external boundary conditions which are needed by the 3D heat transport solver include: (1) the heat flux at the cladding surface, and (2) the temperature or heat transfer coefficient at the crud/coolant interface. The temperature or effective heat transfer coefficient at the crud/coolant interface is computed external to MAMBA (i.e., it is supplied by the CFD code). The heat transfer coefficient can be based on standard forced convection and may also include the effects of sub-cooled boiling at the surface using a Chen or Thom type correlation.[19] More advanced heat transfer models are also being developed within CASL based on two-phase flow and will be implemented as they become available. Sub-cooled boiling within the CRUD layer is modeled by MAMBA. To briefly summarize (a detailed description will be presented elsewhere), a forced convection heat transfer model is used to model the vaporization of the fluid within the pores and exiting via the boiling chimneys in the crud layer. Within each MAMBA computational cell the local heat power density removed due to boiling is given by $q = H_{tc}\ (T - Tsat)$ where Tsat is the local saturation (boiling) temperature of the fluid within the pores. Tsat is a function of the local boric acid concentration and is given by the correlation in Ref. [4]. The temperature T is the local crud temperature and H_{tc} is an empirical heat transfer coefficient which is a function of the local porosity and boiling chimney properties (diameter and density). The boiling heat flux is used as a sink in the 3D non-linear heat transfer calculation and it is also used to compute the local radial Darcy flow velocity within the CRUD. A radial integration through the crud layer is used to compute the total mass evaporation rate exiting the surface of the crud into the coolant. The boiling model in MAMBA has been benchmarked against those used in BOA[18] and successfully validated against recent Westinghouse WALT Loop experiments.[17, 20] More advanced boiling models based on two-phase flow are also under development.

The data exchange between MAMBA and STAR-CCM+ was performed via ASCII data files. The ASCII file generated by STAR-CCM+ and passed to MAMBA includes XYZ tables for the crud layer surface temperature, the cladding surface temperature (below the crud layer), the turbulent kinetic energy in the boundary layer, and the surface heat flux. Since the STAR-CCM+

mesh is much finer than the MAMBA mesh, an efficient surface grid mapping was implemented based on finding the closest STAR-CCM+ node to each MAMBA node. The ASCII file generated by MAMBA and passed to STAR-CCM+ includes a XYZ table for the crud thickness and thermal resistance between cladding surface and coolant introduced by the crud layer. The MAMBA computed XYZ table assigns the same values of crud thickness and thermal resistance to all of the STAR-CCM+ nodes within a given MAMBA surface element (i.e., these variables are passed to STAR-CMM+ at the resolution of the MAMBA mesh). The thermal resistance provided by MAMBA was mapped at the solid-fluid interface using the Star-CCM+ XYZ table tool. A scheme of the coupling data flow is shown in figure 6.

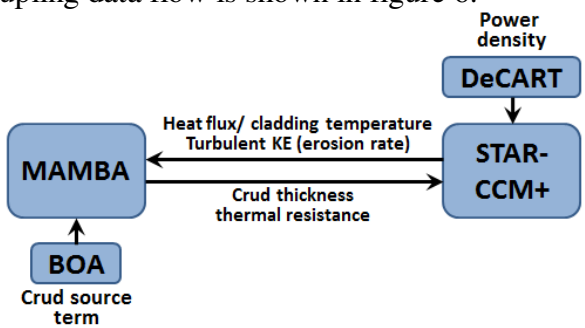

Figure 6 – Coupling scheme with data flow.

3. CALCULATION RESULTS

For the sake of simplifying the description of the results, the fuel pins have been numbered according to the scheme presented in figure 7. The hottest rod in terms of volumetric power (power density) is pin #13 (see also figure 1). The computed cladding temperature is indicated in figure 8; here the effect of the flow swirl induced by the mixing vanes on the temperature distribution can be observed. The cladding temperature can have a significant azimuthal variation, especially after the mixing vanes of the grid spacers. To illustrate this, the azimuthal temperature distribution for selected fuel pins (number 7, 10 and 13 in figure 7) is analyzed. Three axial locations in the proximity of the upper modeled spacer grid are selected: upstream of the mixing vanes (rim 1), in between the vanes (rim 2) and downstream of the vanes (rim 3) respectively (see figure 9). The azimuthal temperature distributions for the selected pins at the specified axial locations are presented in figure 10.

Here the effect of the mixing vanes on the temperature values can be clearly observed. The mixing vanes induce a flow swirl which has the effect of increasing the local heat transfer, with a subsequent decrease of the local cladding temperature, in the region where the coolant flow is accelerated. Different fuel rods in the bundle are affected in a different way by the flow swirl, since the number of mixing vanes surrounding central and peripheral fuel rods is not identical. Remarkably, the cladding peak temperature does not necessarily occur in the hottest pin (# 13). This is because, in addition to the power distribution in the fuel, local coolant effects occurring after the mixing vanes play an important role as well. The azimuthal variations of the turbulent kinetic energy and the shear stress for rods 10 and 13 are reported in figure 11. As mentioned in chapter 2.2, the turbulent kinetic energy was used as a source term for the CRUD erosion model implemented in MAMBA. A physical parameter which would be better correlated to the CRUD erosion is the magnitude of the local shear stress at the wall. However, if a k-epsilon turbulence model is used as in the present simulation, the azimuthal variations of turbulent kinetic energy and shear stress are in-phase and the ratio between the two quantities is practically constant with

exception to a few locations in proximity to spacer grids entry. Therefore, an erosion model based on either of these quantities will provide a very similar CRUD striping pattern. However, a formulation of the erosion term as function of the shear stresses would be more general, in case more advanced turbulence models are employed (e.g. Reynolds stress turbulence models). Therefore, in the future it is planned to correlate the CRUD erosion to the magnitude of the local shear stress.

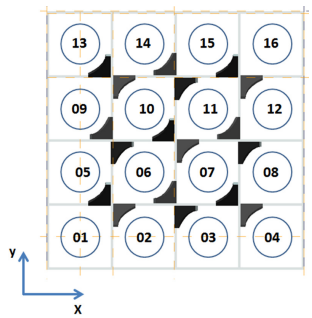

Figure 7 – Fuel pins numbering map.

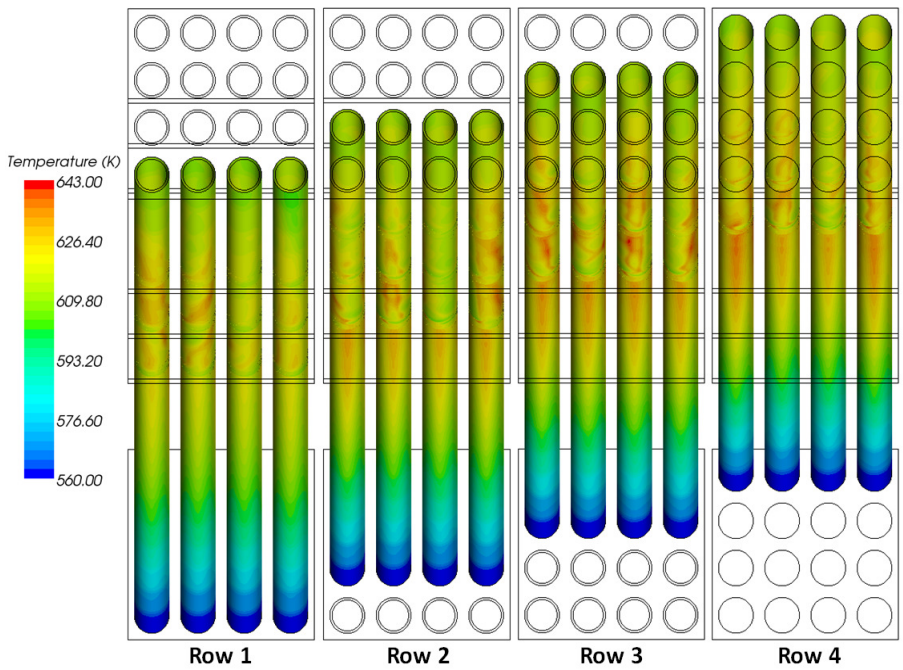

Figure 8 – Cladding temperature for each row of fuel rods.

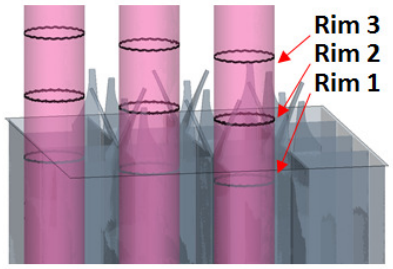

Figure 9 – Reported axial positions.

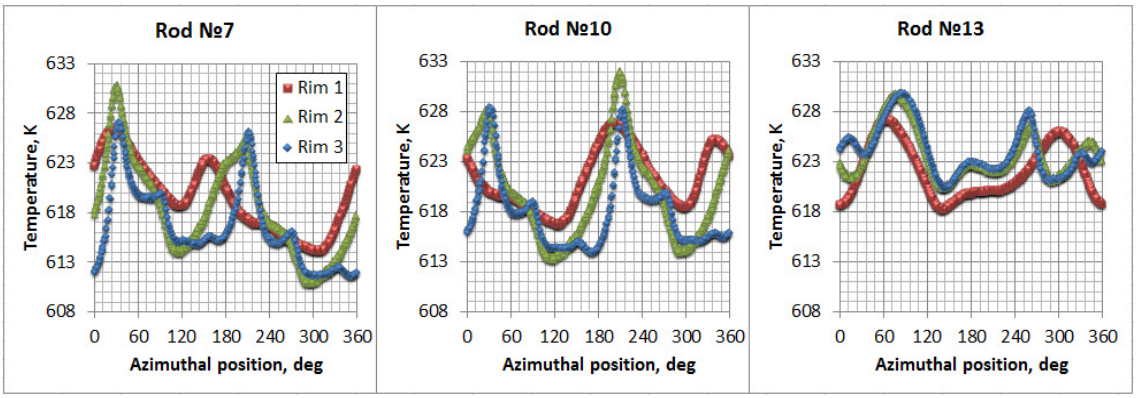

Figure 10 – Azimuthal temperature variation in proximity of third grid spacer.

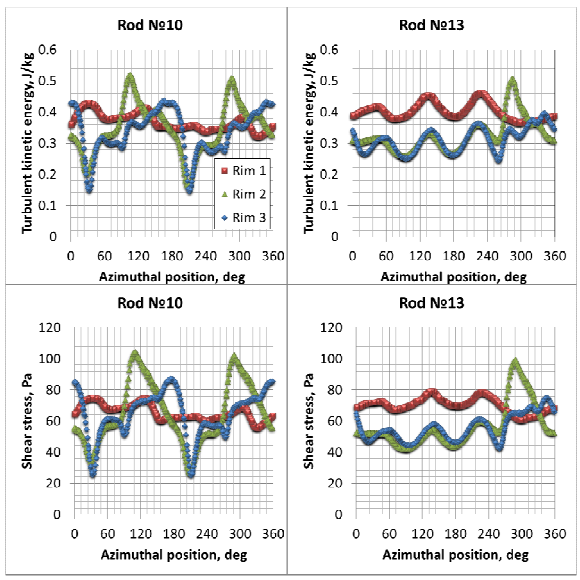

Figure 11 – Turbulent kinetic energy and shear stresses in proximity of third grid spacer.

In order to explore the impact of the erosion term on the CRUD, MAMBA simulations were run for a 300-days cycle, using a fixed set of thermal-hydraulic boundary conditions provided by STAR-CCM+ (cladding surface heat flux, crud/coolant surface temperature, and turbulent kinetic energy). The water chemistry and the crud deposition rates for the boiling and non-boiling regions were chosen to achieve CRUD growth rates and thicknesses similar to those observed in PWRs. The erosion rate (i.e., the constant multiplying the turbulent kinetic energy computed by STAR-CCM+) was also set to qualitatively reproduce the absence of CRUD immediately above the spacer grids, as observed in PWR fuel. A realistic boron let down curve, decreasing from 1400ppm to 535ppm over the 300-days period. The lithium was also adjusted between 2.2 and 2.0 ppm in order to maintain a pH level between 6.8 and 7.25. Simulations were performed with and without the CRUD erosion term. The effect of the erosion on the CRUD and boron mass deposited on the fuel is shown in figure 12 for the three selected pins. As expected, a significant decrease in both the crud and boron mass deposited on the fuel rod surface can be observed if CRUD erosion is not modeled. The boron uptake is especially sensitive to erosion. This sensitivity is due to the non-linear response associated with decreased

boiling within the thinner CRUD layer. The CRUD deposition patterns for each rod are shown in figure 13. The effects of erosion above each spacer grid are clearly visible (horizontal blue "rings"). In addition, CRUD streak deposits can also be observed, caused by the swirling fluid flowing around the pins. These "streak deposits" are similar to those observed in PWRs. A "zoomed in" high-resolution MAMBA simulation was also performed for the region around the first spacer grid (figure 14). The CRUD layer's thermal resistance is plotted in figure 14 along the surface of the pin, and tracks the fluid flow pattern quite well. In the lower resolution (full pin) MAMBA simulations, the minimum CRUD thickness did not always correspond exactly to the locations of maximum turbulent kinetic energy. The higher resolution simulation verified that this artifact was due to the lower resolution mesh, which was chosen for the full pin simulations as a compromise between fidelity and computational cost.

Additional investigations performed by changing the MAMBA mesh size have shown that a smoother and more physical profile of the CRUD layer is easily achievable by reducing the cells size closer to the order of cell size used in CFD mesh, as shown in figure 14.

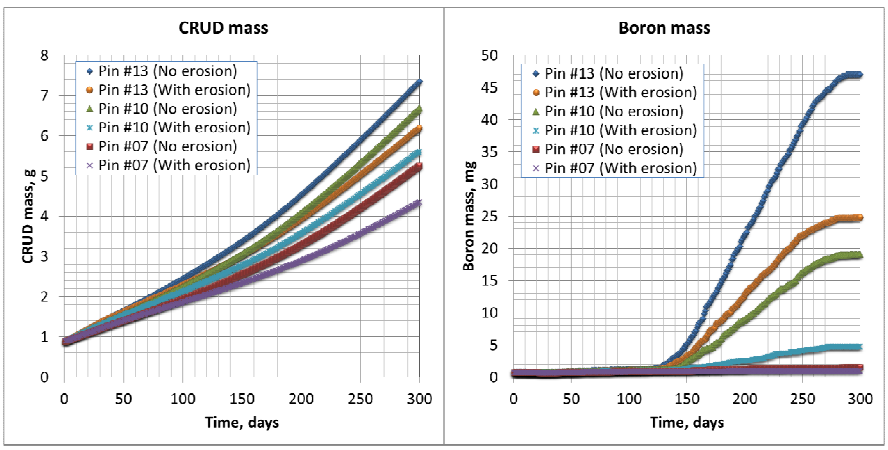

Figure 12 – Total CRUD mass (left), boron mass (right).

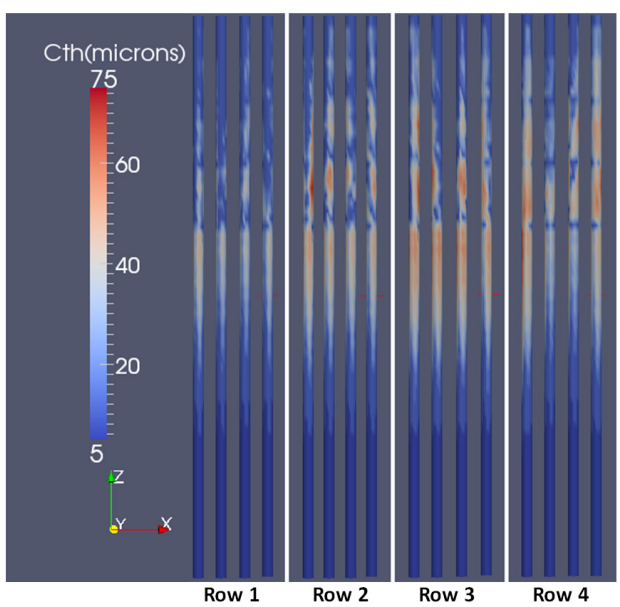

Figure 13 – CRUD formation on fuel rods.

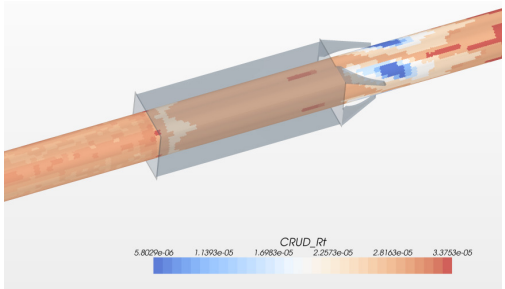

Figure 14 – high MAMBA mesh resolution

4. CONCLUSION

This study demonstrates that a high-fidelity coupled treatment of CRUD deposition and CFD is required in order to accurately model the deposition of CRUD at the pin scale. In particular, significant azimuthal variations in the fluid flow especially in the regions near the spacer grids lead to CRUD streak deposits consistent with those observed in PWRs. The variations in the CRUD thickness are due to both flow-induced surface erosion and thermal hydraulic effects. The sensitivity of the total CRUD and boron mass deposited on each pin with respect to erosion demonstrates the need for more advanced and validated erosion models. Significant pin-to-pin variations in crud mass and boron uptake were also observed due to the variations in the pin power across the 4x4. These large variations show that the correct pin level power density must be used as the boundary conditions for the CFD calculation. The effect of computational mesh resolution must also be systematically investigated in order to verify convergence of the total CRUD and boron mass deposited, as well as its axial and azimuthal distribution along the pin. Future work will include a two-way coupled calculation between MAMBA and STAR-CCM+ and the incorporation of more advanced erosion models based on local shear stresses. High fidelity pin scale modelling of CRUD deposition is especially important for identifying potential "hot spots" on the cladding surface which have increased risk for CILC.

REFERENCES

[1] G.C.W. Comley, The significance of corrosion products in water reactor coolant circuits, Progress in Nuclear Energy, Volume 16, Issue 1, 1985, Pages 41-72

[2] P. Cohen, Heat and mass transfer for boiling in porous deposits with chimneys, AICHE Symposium Series 70, 71-80, (1974).

[3] R. Castelli, Nuclear corrosion modeling: the nature of crud, Elsevier Inc., Burlington, MA, USA (2010).

[4] J. Deshon, PWR axial offset anomaly (AOA) guidelines, revision 1. Technical Report 1008102, EPRI, Palo Alto, CA, 2004 (and references therein).

[5] J. Deshon, Modeling PWR fuel corrosion product deposition and growth process. Technical Report 1011743, EPRI, Palo Alto, CA, 2005.

[6] B. Jones, et. al., Modeling and thermal performance evaluation of porous crud layers in sub-cooled boiling region of PWRs and effects of sub-cooled boiling on anomalous porous crud deposition on fuel pin surfaces, DOE report DEFG07-00ID13924 (2005).

[7] J. Deshon, D. Hussey, B. Kendrick, J. McGurk, J. Secker, M. Short, Pressurized water reactor fuel crud and corrosion modeling, Journal of Materials, August 2011, Volume 63, Issue 8, Pages 64-72 (and references therein).

[8] J.A. Sawicki, Analyses of crud deposits on fuel rods in PWRs using Mössbauer spectroscopy, Journal of Nuclear Materials, Volume 402, Issues 2–3, 31 July 2010, Pages 124-129.

[9] P.L. Frattini, T. Moser, The ultrasonic key to clean fuel, Water Chemistry of Nuclear Reactor Systems 8: Proceedings of the Conference Organized by the British Nuclear Energy Society and Held in Bournemouth, UK, on 22-26 October 2000, Pages 457-458.

[10] Kochunas B., Stimpson, S., Collins, B., Downar, T., Brewster, R., Baglietto, E., 2012. Coupled Neutron Transport/CFD simulations of whole core pressurized water reactor. Proc. of Int. Conf. On Advances in Reactor Physics, PHYSOR 2012, Knoxville, Tennessee, USA, April 15 - 20.

[11] Navarro, M.A., Santos, A.A.C., 2011. Evaluation of a numeric procedure for flow simulation of a 5x5 PWR rod bundle with a mixing vane spacer, Progress of Nuclear Energy, 53, pp. 1190-1196.

[12] Linstrom, P.J.; Mallard, W.G. (eds.) NIST Chemistry WebBook, NIST Standard Reference Database Number 69. National Institute of Standards and Technology, Gaithersburg MD. http://webbook.nist.gov.

[13] STAR-CCM+ User guide, v7.04, CD-adapco, (2012).

[14] J.W. Cleaver and B.Yates, The effect of reentrainment on particle deposition. Chem. Eng. Sci. 31, 147-151 (1976).

[15] B.P.K. Yung, H. Merry, and T.R. Bott, The role of turbulent bursts in particle reentrainment in aqueous systems, Chem. Eng. Sci. 44, 873-882, (1989).

[16] J.D. Nelligan, N. Kallay, and E. Matijevic, Particle Adhesion and removal in model systems, J. Colloid Interface Sci. 89, 9-15 (1982).

[17] J. Deshon, G. Wang, A. Byers, and M. Young, Simulated fuel crud thermal conductivity measurements under pressurized water reactor conditions. Technical Report 1022896, EPRI, Palo Alto, CA, 2011.

[18] Boron-Induced Offset Anomaly (BOA) Risk Assessment Tool, Version 1.0 (Palo Alto, CA: EPRI, 2003), 1003211.

[19] K.E. Gungor and R.H.S. Winterton, A general correlation for flow boiling in tubes and annuli, Int. J. Heat Mass Transfer 29, 351-358 (1986).

[20] B.K. Kendrick and J. Barber, Initial validation and benchmark study of 3D MAMBA v2.0 against the WALT loop experiment and BOA v3.0, internal CASL report MPOCRUD.P5.02, August 10, 2012.